PHYSICAL REVIEW B **79**, 214431 (2009)

Far-infrared optical study of electromagnons and their coupling to optical phonons in $Eu_{1-x}Y_xMnO_3$ ($x=0.1$, 0.2, 0.3, 0.4, and 0.45)

Y. Takahashi,[1] Y. Yamasaki,[2] N. Kida,[1] Y. Kaneko,[1] T. Arima,[3] R. Shimano,[1,4] and Y. Tokura[1,2,5]
[1]*Multiferroics Project, ERATO, Japan Science and Technology Agency (JST), c/o Department of Applied Physics, The University of Tokyo, Tokyo 113-8656, Japan*
[2]*Department of Applied Physics, The University of Tokyo, Tokyo 113-8656, Japan*
[3]*Institute of Multidisciplinary Research for Advanced Materials, Tohoku University, Sendai 980-8577, Japan*
[4]*Department of Physics, The University of Tokyo, Tokyo 113-0033, Japan*
[5]*Cross-Correlated Material Research Group (CMRG), ASI, RIKEN, Wako, Saitama 351-0198, Japan*
(Received 27 April 2009; revised manuscript received 3 June 2009; published 24 June 2009)

A systematic far-infrared optical study has been performed on multiferroic oxides $Eu_{1-x}Y_xMnO_3$ ($x=0.1$, 0.2, 0.3, 0.4, and 0.45) in which versatile characteristics of magnetic orders including the *ab*- and *bc*-plane spiral, *A*-type antiferromagnetic, and collinear sinusoidal states show up, depending on Y content (x) and temperature. We have observed evolution of various absorption bands below 100 cm^{-1}, which critically depends on the nature of magnetic order and hence can be assigned to magnetic excitations. The spiral-spin structures yield the most intense absorption composed of two pronounced peak structures around 20 and 65 cm^{-1}, while the spectra for the collinear sinusoidal spin structure exhibit a plateaulike shape below 80 cm^{-1}. In contrast, the *A*-type antiferromagnetic phase shows no electrically active spin excitation. A quantitative analysis shows their strong mutual coupling in the spiral-spin phases as manifested by the transfer of the spectral weight between the electrically active spin excitations and the lowest optical-phonon mode.

DOI: 10.1103/PhysRevB.79.214431 PACS number(s): 75.80.+q, 76.50.+g, 75.40.Gb

I. INTRODUCTION

Since the recent discovery of the magnetoelectric multiferroicity in $TbMnO_3$,[1] materials with cross-correlated electric and magnetic properties have attracted renewed attention because of their novel magnetoelectric phenomena as well as possible applications.[2] The orthorhombic $RMnO_3$ (R=Tb, Gd, Dy, or $Eu_{1-x}Y_x$) with perovskite-like structure undergoes a ferroelectric transition induced by the transverse-spiral-spin (cycloidal-spin) structure, and the application of external magnetic field gives rise to a flop in the direction of spontaneous polarization ($\vec{P}_s$).[1,3] This interplay can be explained by inverse Dzyaloshinski-Moriya (IDM) mechanism;[4–6] the microscopic polarization $\vec{P}_s$ is expressed as $\vec{P}_s \propto \vec{e}_{ij} \times (\vec{S}_i \times \vec{S}_j)$ for a pair of spins $\vec{S}_i$ and $\vec{S}_j$ with a unit vector $\vec{e}_{ij}$ connecting them and, accordingly, the cycloidal-spin order can produce the macroscopic (spontaneous) polarization directing perpendicular to the magnetic modulation vector $q_m(\|\vec{e}_{ij})$ and parallel to the spiral-spin plane. Indeed, the change in the spin helicity (the sign of $\vec{S}_i \times \vec{S}_j$) due to the reversal of the spontaneous polarization ($\vec{P}_s$) has been confirmed for the *bc*-spiral phase in $TbMnO_3$ and for the *ab*-spiral phase in $Gd_{0.7}Tb_{0.3}MnO_3$ by polarized neutron scattering.[7,8] Such strong interplay between ferroelectricity and magnetism may lead to the presence of low-energy excitations composed of both electric and magnetic characters. The possibility of such excitation, termed *electromagnon*, has been first proposed experimentally for $TbMnO_3$ and $GdMnO_3$ by Pimenov *et al.*[9] as infrared absorption around 20 cm^{-1}. Since the lower-edge absorption band is close to the energy of the magnon at $q=q_m$ observed by inelastic neutron scattering,[10,11] the origin of the observed electromagnon was attributed to a rotary oscillation mode of the spiral-spin plane, i.e., the Nambu-Goldstone mode for the spontaneous polarization as expected theoretically by the IDM mechanism.[12] Indeed, the polarization-selection rule seemed to satisfy the above interpretation in an early study[9–11] in which electromagnon should be active for $E^{\omega}\|a$ in case of the *bc*-spiral plane. However, ensuing investigations on a series of $RMnO_3$ [$Eu_{1-x}Y_x$,[13,14] $Gd_{1-x}Tb_x$,[15–17] and $Tb_{1-x}Dy_x$,[17]] have revealed that the electromagnon is active only for $E^{\omega}\|a$, irrespective of the direction of ferroelectric polarization, which is directly identical in $DyMnO_3$ by controlling the direction of the spiral-spin plane (*bc* to *ab*) with the applied magnetic field.[15,18] Recent terahertz and Fourier-transform infrared (FTIR) spectroscopies have further revealed a new generic feature that the electric-dipole active magnetic-excitation band consists of two peaks around 20 and 60 cm^{-1}, of which the higher-lying peak is close to the energy of the zone-edge magnon.[13,15–20] It has recently been theoretically proposed that the exchange striction arising from the $\vec{S}_i \cdot \vec{S}_j$ term in the noncollinear-spin state, instead of IDM mechanism, could give rise to such electric-dipole active magnetic (one-magnon) excitations corresponding to the zone-edge magnon,[20,21] while the origin of the lower-energy mode is still unresolved. (Here note that the zone-edge mode should be folded by the cycloidal spin order to bear the $k=0$ component.) Another important feature to understand the origin of the electromagnons is its coupling with phonons. A clear correlation between the electromagnon and phonon has been observed in $GdMnO_3$,[22] $TbMnO_3$,[19] and $Eu_{0.75}Y_{0.25}MnO_3$,[13] which shows up as a frequency shift in the lowest-lying optical phonon or a transfer of spectral weight from this optical phonon to the electromagnon and/or electric-dipole active magnetic-excitations band, suggesting the dynamical magnetoelectric coupling. In this paper, the term electromagnon is used for well-defined one-particle ex-

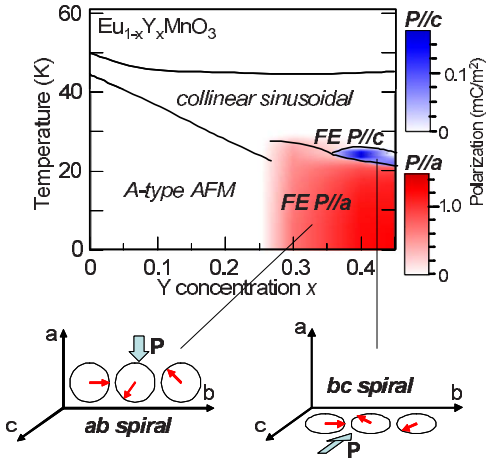

FIG. 1. (Color online) The phase diagram of $Eu_{1-x}Y_xMnO_3$ reproduced from Refs. 23 and 24. The regions, denoted by FE P//a (red online) and FE P//c (blue online), indicate the observed magnitude of polarization for $\vec{P}_s \| a$ and c (see the color code on the right panel). The schematic of spin structures and directions of $\vec{P}_s$ in *ab*- and *bc*-plane transverse-spiral-spin (cycloidal) state in orthorhombic setting are also shown in the lower panel.

citations as identified by the peak structure. On the other hand, we use the term electric-dipole active magnetic excitation more generally including electromagnons and also the continuumlike excitation band, which is mainly observed in the collinear sinusoidal spin phase.

Among the orthorhombic rare-earth manganites, the solid solution $Eu_{1-x}Y_xMnO_3$ can provide a simple situation for the systematic investigation on electromagnons and/or electric-dipole active magnetic excitations with the variation in Mn spin alone due to the absence of the magnetic *f* moment for Eu^{3+} and Y^{3+}. Figure 1 shows the phase diagram of $Eu_{1-x}Y_xMnO_3$ in the plane of temperature vs Y concentration *x*.[23,24] In the low $x(<0.25)$, the material undergoes the successive magnetic-phase transitions to the collinear sinusoidal state (at $T_N^{\mathrm{Mn}}=46$ K for $x=0.2$) and then to the *A*-type antiferromagnetic (AFM) one (at $T_N^{\mathrm{WFM}}=28$ K for $x=0.2$) with decreasing temperature due to the competition between ferromagnetic nearest-neighbor superexchange interaction J_1 and antiferromagnetic next-nearest-neighbor interaction J_2 in the *ab* plane.[25,26] With increasing $x(>0.25)$, the magnitude of J_2 and hence the magnetic frustration are further enhanced. Then, the *A*-type AFM phase is no more present as the ground state and changes into the *ab*-spiral phase which is accompanied by emergence of spontaneous polarization along the *a* axis. This system also undergoes the *bc*-spiral phase, which hosts $\vec{P}_s \| c$, in the intermediate temperature region for $x>0.4$ ($T_{c2}=24$ K$<T<T_{c1}=26$ K at $x=0.4$). The rotation of $\vec{P}_s$ under rotating magnetic field in $Eu_{0.55}Y_{0.45}MnO_3$ has been demonstrated and readily explained by taking into account the rotation of conical spiral-spin structure.[27] This is in contrast to the case of $TbMnO_3$, which shows the complicated phase diagram under application of magnetic fields due to the presence of *f* moment of Tb^{3+} ions.[28] The phase diagram for $Eu_{1-x}Y_xMnO_3$, including the thermally induced flop of spiral plane and the appearance of the collinear sinusoidal and *A*-type AFM phase, can be quantitatively reproduced by the Heisenberg-model calculation with the realistic parameterization of exchange interactions and magnetic anisotropy.[26] Accordingly, the systematic terahertz or far-infrared spectroscopy on $Eu_{1-x}Y_xMnO_3$ enables us to map the electromagnon and/or electric-dipole active magnetic-excitations characteristics on to the versatile phase diagrams including four different magnetic orders: collinear sinusoidal, *ab*-plane spiral, *bc*-plane spiral, and *A*-type AFM. Although the low-energy spectra only below 40 cm^{-1} for $x=0$, 0.1, 0.2, 0.3, 0.4, and 0.5 as well as the spectrum including the lowest optical phonon mode for $x=0.25$ (subtly close to the phase boundary, see Fig. 1) have been reported so far (Refs. 13 and 14), full investigation on the optical spectra and correlation of electromagnon and/or electric-dipole active magnetic excitations and phonons will further provide useful information on the unresolved nature of electromagnon excitations and their systematics in multiferroic perovskite manganites. Here we show the results of far-infrared optical spectroscopy on $Eu_{1-x}Y_xMnO_3$ with systematically changing *x* as $x=0.1$, 0.2, 0.3, 0.4, and 0.45. The spectra of electromagnons and/or electric-dipole active magnetic excitations, as well as the shift in their peak positions, were observed to critically depend on the magnetic orders. The lowest optical-phonon mode coupled with electromagnon and/or electric-dipole active magnetic excitations was also quantitatively investigated to argue the contribution of the lattice dynamics.

II. EXPERIMENT

Single crystals of $Eu_{1-x}Y_xMnO_3$ with $x=0.1$, 0.2, 0.3, 0.4, and 0.45 were grown by a floating-zone method.[24] We performed terahertz time-domain spectroscopy in transmission configuration to determine both the real and imaginary parts of the complex dielectric constant from 13 to 80 cm^{-1}. The detailed experimental setup and the analysis procedure are described in Ref. 18. The terahertz wave was generated by the optical rectification of an ultrashort laser pulse in a ZnTe(110) crystal and detected by a dipole antenna.[29] From the measured complex transmittance spectrum, we determined the complex optical constant $\tilde{n}^2=\tilde{\epsilon}\tilde{\mu}$, where the $\tilde{\epsilon}$ and $\tilde{\mu}$ are complex dielectric and magnetic permittivity, respectively. In the analysis, we assume that $\tilde{\mu}-1$ is small in absolute magnitude and that its effect on the Fresnel coefficient is negligible. The validity of this assumption was checked as described in Ref. 18. For the frequency (photon energy) range form 80 to 650 cm^{-1}, we conducted both reflection and transmission FTIR measurements. The samples were polished to 20–50 μm in thicknesses for the transmission measurement with FTIR. We determined the complex dielectric constant using both reflectance and transmittance data in the energy range from 80 to 180 cm^{-1} without resorting to the Kramers-Kronig analysis.

III. POLARIZATION AND *x* DEPENDENCE OF ELECTROMAGNON SPECTRA

Figure 2 shows spectra of the real and imaginary parts of the dielectric constant (below 80 cm^{-1}) with all independent

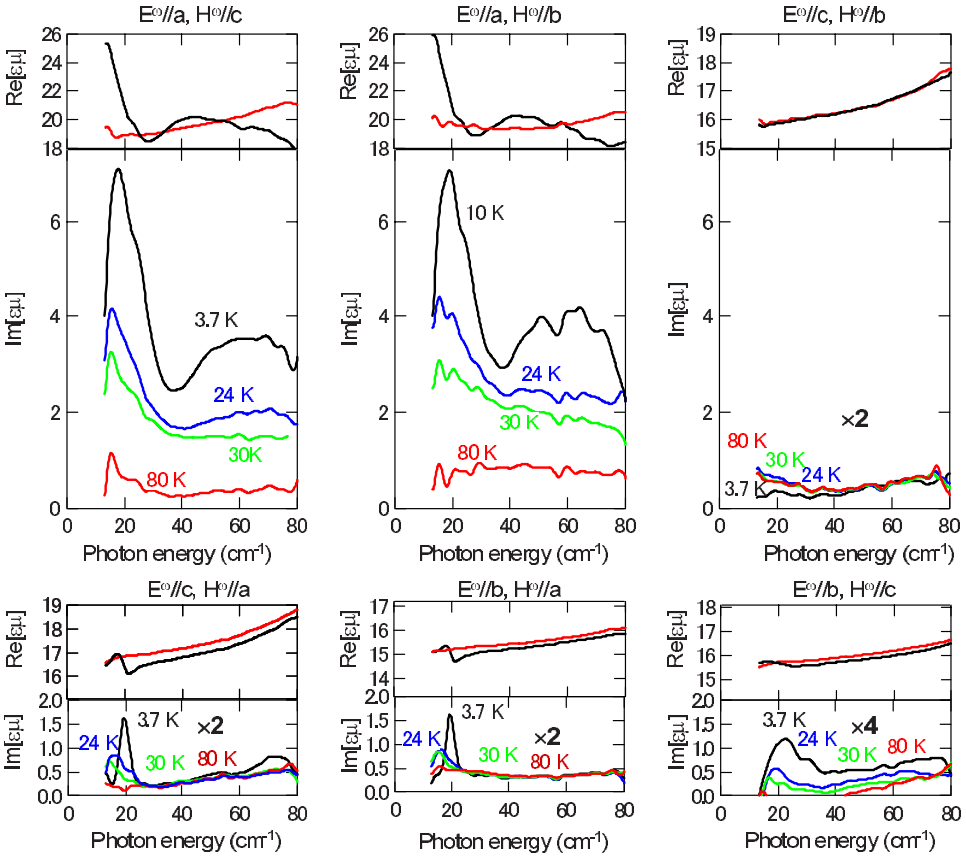

FIG. 2. (Color online) Re[$\epsilon\mu$] and Im[$\epsilon\mu$] spectra for $Eu_{1-x}Y_xMnO_3$(x=0.45) at various temperatures in all polarization (E^ω,H^ω) configurations of light. E^ω and H^ω represent electric and magnetic fields of light, respectively.

light-polarization configurations (in the orthorhombic-lattice setting) for x=0.45. At 24 K and lower temperatures (3–10 K), where the *bc*-spiral- and the *ab*-spiral-spin order occur, respectively, a strong absorption band is observed in $E^\omega \| a$ configurations ($H^\omega \| b,c$); this indicates that the magnetic order gives rise to the electrically active excitation in $E^\omega \| a$ configuration irrespective of the direction of spontaneous polarization ($\vec{P}_s \| a$ or c axis). The spectra with the two peaks at 19 and 60 cm^{-1} develop in the spiral-spin phase, while a plateaulike absorption band is identified in the collinear sinusoidal phase (30 K). The same trend is also observed for x =0.4 and 0.3, while accompanied by the shifts in the peak positions in the spiral-spin phase, as shown in Fig. 3. These results are consistent with the observations for other $RMnO_3$ in which the electrically active magnetic excitations have also been observed for $E^\omega \| a$.[9,13–20] In other polarization configurations, the magnetic excitations activated by H^ω component appear for $H^\omega \| a(E^\omega \| b,c)$ and for $H^\omega \| c(E^\omega \| b)$ around 20 cm^{-1}, as manifested by the sharp peaks in Im[$\epsilon\mu$] and the dispersive structure in Re[$\epsilon\mu$] (Fig. 2). Hereafter, we focus on the spectra in the $E^\omega \| a$ configuration, in which electric-dipole active magnetic excitations including electromagnons can show up.

Figure 3 shows the $E^\omega \| a$ spectra for x=0.1, 0.2, 0.3, 0.4, and 0.45. A large difference can be seen between the spectra for $x \geq 0.3$ and ≤ 0.2 at the lowest temperature. With changing x, the magnetic ground state undergoes the transition between the *A*-type AFM (x=0.2) and the *ab*-spiral (x =0.3) phase, as shown in Fig. 1. In the *A*-type AFM state (x=0.1 and 0.2), the characteristic electromagnon band ($E^\omega \| a$) totally disappears. On the other hand, a plateaulike broad band is identified even for x=0.1 and 0.2 in the collinear sinusoidal phase at 40 and 30 K, respectively. Thus the electrically active magnetic excitations may be characterized according to three kinds of magnetic orders. The strongest electromagnon with a two-peak feature appears in the *ab*- and *bc*-plane spiral-spin phases as observed for x=0.3, 0.4, and 0.45. The plateaulike broadband structure is observed in the collinear sinusoidal phase for all the compositions. In the *A*-type AFM phase, there is no electrically active spin excitation, while the sharp absorption peaks (responding to $H^\omega \| c$) are clearly identified at 20 cm^{-1} for x=0.1 and 0.2. This excitation in the *A*-type AFM state has been assigned to the antiferromagnetic resonance for $Eu_{1-x}Y_xMnO_3$,[14]) and for $Gd_{0.7}Tb_{0.3}MnO_3$.[16]

Next we show the correlation between the spectral weights of the lowest optical phonon and the electromagnons. In the lower-energy region, a pair of phonon modes located around 120 and 160 cm^{-1} are observed for all the compositions and can be ascribed to the external mode, which mainly come from the vibration of the rare-earth ions. Due to the large difference in mass between Eu (152) and Y (89), this external mode shows the persistent-type behavior in the mixed crystals, resulting in it splitting into two modes. Indeed the frequencies of these phonons are not sensitive to x, as shown in Fig. 4. The intensity of the lower-lying Eu mode at 120 cm^{-1} markedly decreases in the collinear and/or spiral-spin phase in x=0.3, 0.4, and 0.45, as shown in Fig. 3. For x=0.1 and 0.2, the intensity of this mode also decreases in the collinear phase but recovers in the *A*-type AFM phase. This behavior is anticorrelated with that of the

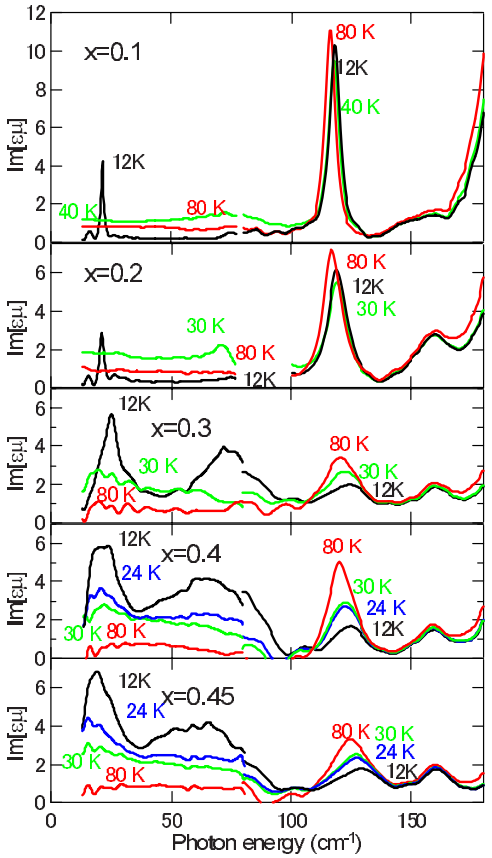

FIG. 3. (Color online) The $E^{\omega}\|a$ Im$[\epsilon\mu]$ spectra for $Eu_{1-x}Y_xMnO_3$ with $x=0.1$, 0.2, 0.3, 0.4, and 0.45 at various temperatures.

electrically active magnetic excitations suggesting that the spectral weight of the phonon mode is transferred to the electromagnon in the spiral-spin phase or to some relevant electrically active magnetic excitations in the collinear sinusoidal spin phase. We will quantitatively discuss this issue later.

The x dependence of the peak positions of $E^{\omega}\|a$ electromagnon and $H^{\omega}\|(a,c)$ magnon modes is shown in Fig. 4. The higher-lying electromagnon peak located at 73 cm^{-1} for $x=0.3$ shifts to 58 cm^{-1} for $x=0.45$. The lower-lying peak also shows a shift from 25 to 19 cm^{-1} with increasing x

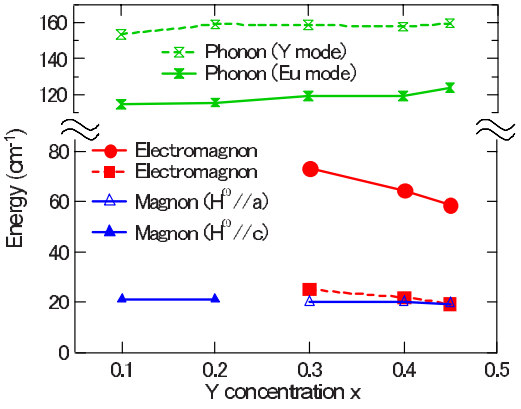

FIG. 4. (Color online) x dependence of energies of phonon, magnon, and electromagnon in $Eu_{1-x}Y_xMnO_3$.

from 0.3 to 0.45. In contrast, the position of the $H^{\omega}\|a$ magnon mode observed in the ab-spiral phase shows little dependence on x. For $x=0.1$ and 0.2, a magnon mode is also identified in the A-type AFM phase at 21 cm^{-1} for $H^{\omega}\|c$ as in the case for $Gd_{0.7}Tb_{0.3}MnO_3$.[16]

IV. TEMPERATURE DEPENDENCE OF ELECTROMAGNON AND OPTICAL PHONON

Temperature dependence of the far-infrared absorption spectra for two representative materials of $x=0.2$ and 0.4 are shown in Fig. 5. At 100–250 K, both materials are nearly transparent below 100 cm^{-1} and only two phonons are observed at 120 and 160 cm^{-1} with a tail of the higher-lying phonon modes. On decreasing temperature to around 50 K, the broad plateaulike absorption band appears in both the materials, while the intensity of phonon around 120 cm^{-1} (B) is gradually decreased. This broad absorption, perhaps of magnetic origin, continues to increase in the collinear sinusoidal phase with further decreasing temperature until the distinct lower-temperature ferroelectric spiral-spin phase appears, as shown in Figs. 5(a) and 5(b). In the spiral-spin phase of $x=0.4$, the absorption is further enhanced, forming the peak-shape characteristic of the electromagnon as also observed also in the spiral-spin phases of other $RMnO_3$. In contrast, the absorption band of $x=0.2$ reaches maximum at 30 K in the collinear sinusoidal phase and then rapidly decreases in the A-type AFM phase where the sharp magnetic resonance arising from the H^{ω} excitation appears in turn at 21 cm^{-1}. Simultaneously, the phonon intensity recovers in the A-type AFM phase below $T_N^{\mathrm{WFM}}=28$ K, evidencing that the spectral weight of the electrically active magnetic excitations originates substantially from the coupling with the lowest phonon mode.

For more quantitative discussion, we estimate the integrated spectral weight per Mn site as given by

$$N_{\mathrm{eff}} = \frac{2m_0V}{\pi e^2}\int_{\omega_1}^{\omega_2} \omega' \,\mathrm{Im}[\tilde{\epsilon}\tilde{\mu}(\omega')]d\omega', \qquad (1)$$

where m_0, e, and V are the bare electron mass, the charge, and the unit-cell volume, respectively. According to the respective spectral ranges, we have deduced the N_{eff} for the electromagnon (or electrically active magnetic-excitation band), the lowest phonon, and the magnon (in A-type AFM phase). For example, $N_{\mathrm{eff}}(T)$ of the electromagnons or electric-dipole active magnetic excitations (A in Fig. 5) is defined as the increase in spectral weight between $\omega_1=13$ and $\omega_2=100$ cm^{-1} from 100 K to eliminate the nonmagnetic contributions. To determine $N_{\mathrm{eff}}(T)$ of the phonon modes, we fitted the spectra with three Lorentz oscillators representing the lowest phonon (B: Eu mode), the second lowest phonon (C: Y mode), and the tail of the higher-lying phonons, respectively. $N_{\mathrm{eff}}(T)$ of the lowest phonon was defined by integrating the thus obtained Lorentz function. $N_{\mathrm{eff}}(T)$ of magnon was also determined from the fitting by a Lorentz oscillator.

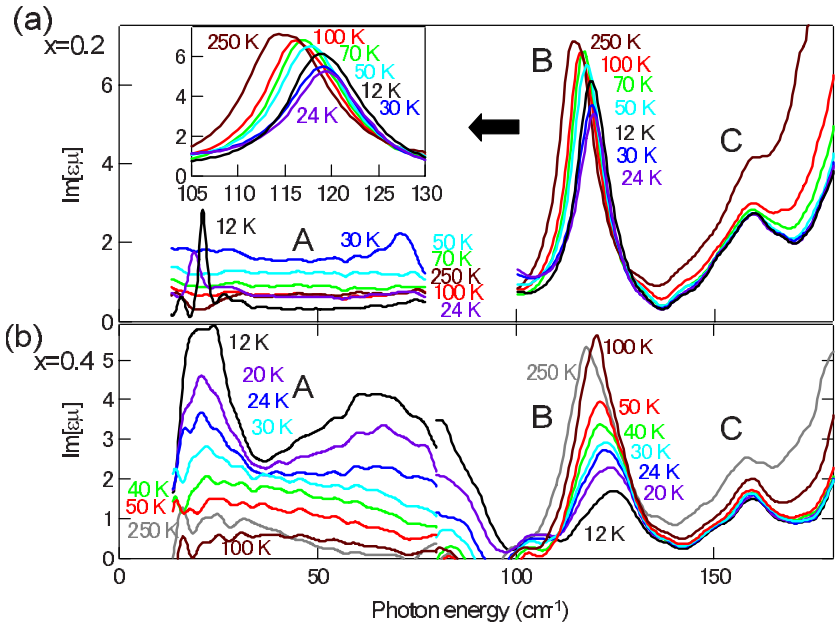

FIG. 5. (Color online) Temperature dependence of $\mathrm{Im}[\epsilon\mu]$ spectra in $E^{\omega}\|a$ for (a) $x=0.2$ and (b) 0.4. The electromagnon (or electrically active magnetic-excitation band) and two lower-lying phonon modes are denoted as A, B, and C, respectively.

Figure 6 shows the temperature dependence of $N_{\mathrm{eff}}(T)$ of electromagnon (or electric-dipole active magnetic excitation) and the lowest phonon for $x=0.2$ and 0.4. The $N_{\mathrm{eff}}(T)$ of the magnetic part (A) develops even in the paramagnetic phase (>46 K) with decreasing temperature in both the compounds. The $N_{\mathrm{eff}}(28\ \mathrm{K})$ in the collinear sinusoidal phase is comparable for $x=0.2$ (0.83×10^{-5}) and 0.4 (0.78×10^{-5}). In contrast, the intensity of the phonon mode B shows a significant difference; relative reduction of 35% and 19% for $x=0.4$ and 0.2 at 28 K, respectively. These results indicate that the strong coupling between the lowest optical phonon and the electric-dipole active magnetic excitation in the collinear sinusoidal phase emerges only for the higher-x compounds

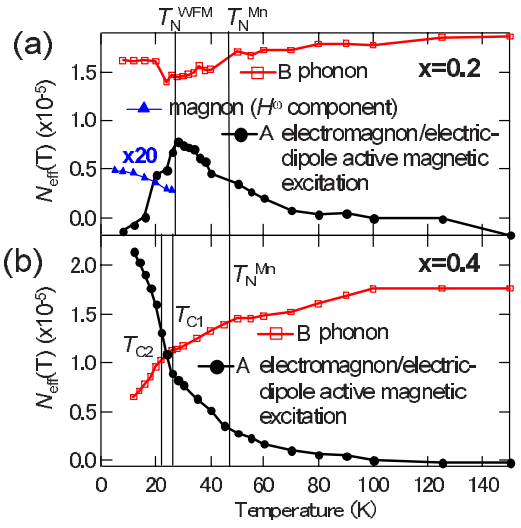

FIG. 6. (Color online) Temperature dependence of spectral weight (N_{eff}, see text for the definition) of (a) the electromagnon (or electric-dipole active magnetic excitation) band and (b) the lower-lying phonon mode for $x=0.2$ (a) and 0.4 (b). (see also Fig. 5). The spectral weight of the magnetic part A is defined as the variation from the value at $T=100$ K.

which undergo the successive transition to the spiral-spin phase, not to the A-type phase. In $x=0.4$, the spectral weight of the magnetic part A is further enhanced, while the phonon intensity (B) is rapidly decreased, below T_{c1}(=26 K). Although the spiral-spin plane flops from bc ($\vec{P}_s\|c$) to ab ($\vec{P}_s\|a$) at T_{c2}=24 K for $x=0.4$, no distinct feature is observed at the point. The spectral weight of the phonon B compensates for 52% of the spectral weight of electromagnon at 12 K. In the case of $Eu_{0.75}Y_{0.25}MnO_3$($x=0.25$),[13] and $TbMnO_3$,[19] which have ab- and bc-spiral ground states, respectively, about 30% of spectral weight of electromagnon appears to be transferred from the lowest phonon mode. On the other hand, the disappearance of the magnetic part A coincides with the recovery of the phonon (B) intensity below T_N^{WFM}(=28 K) in $x=0.2$, as shown in Fig. 6(a). In the A-type AFM phase, there is no strong electric-dipole active excitation in the energy range of magnetic excitations, while development of the H^{ω}-induced antiferromagnetic resonance is discerned with decreasing temperature. In accord with this, the phonon spectral weight shows a slight recovery upon the transition to the A-type AFM state.

V. DISCUSSION

To investigate the systematic dependence of the coupling between the electrically active magnetic excitations and the lowest phonon, we show in Fig. 7 the temperature dependence of the spectral weights of the magnetic part (A) and the phonon mode (B) for the respective compounds. The spectral weight of the lowest phonon mode is normalized by the value at 100 K. The corresponding contour color plots of the respective spectral weights of the lowest phonon and the electromagnon/electrically active magnetic excitation are displayed on the phase diagram in Fig. 8. Phase diagrams shown in Figs. 8(a) and 8(b), as coded with the respective spectral weights, show a complementary landscape suggesting a strong anticorrelation between the lowest optical pho-

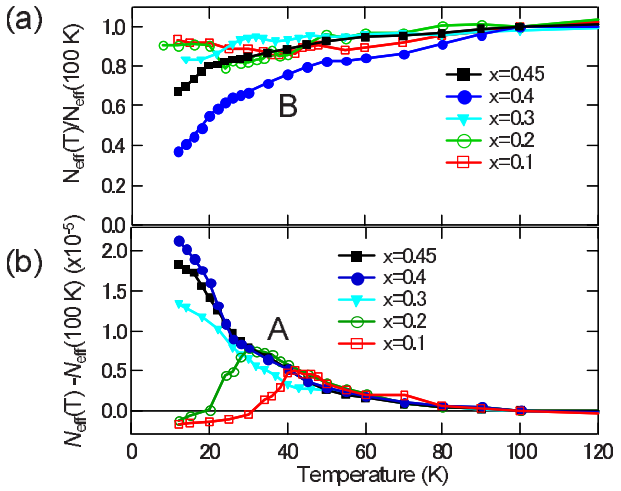

FIG. 7. (Color online) (a) Temperature dependence of spectral weight $N_{\mathrm{eff}}(T)$ of the phonon mode B as normalized by the respective values at 100 K for each composition (x). (b) Temperature dependence of spectral weight $N_{\mathrm{eff}}(T)$ of the magnetic part A (electromagnon or electric-dipole active magnetic-excitation band) defined as the variation from the respective values at $T=100$ K.

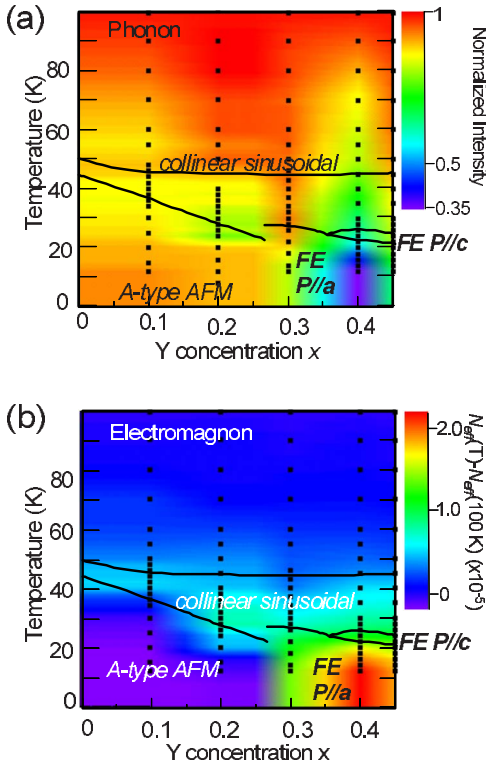

FIG. 8. (Color online) The contour mapping of (a) the normalized phonon mode B intensity [Fig. 7(a)] and (b) the spectral weight of the magnetic part A [Fig. 7(b)] on the phase diagram. The dots indicate the data-acquisition points. The color contour was obtained by linear interpolation from these data points. As for the values at $T=0$ K, we used the values obtained at the lowest temperature ($\sim$10 K), assuming that the ground state is identical with the state at $\sim$10 K.

non and electromagnon and/or electric-dipole active magnetic excitations. The strongest electromagnon appears in the spiral-spin phase accompanied by the remarkable suppression of the phonon intensity. On the other hand, a certain amount of electric-dipole active absorption for magnetic excitations appears even in the paraelectric collinear sinusoidal phase of $x=0.1$ and 0.2. The disappearance of the electromagnon absorption band in the A-type AFM phase is well contrasted with the strong absorption due to the electromagnon in the spiral-spin ferroelectric phase, as seen in the phase boundary around $x=0.25$ in Fig. 8(b). As shown in Fig. 7, one half of the spectral weight of electromagnon appears to be transferred from the lowest optical-phonon mode for the case of $x=0.4$ at the lowest temperature. The residual part of the spectral weight should originate from the higher-lying phonons and/or electronic excitation.

The mechanism of the strong dipole activity of electromagnon is a controversial issue. Two intense peaks around 20 and 60 cm^{-1} are clearly observed in the spiral-spin phase for $x=0.3$, 0.4, and 0.45. As mentioned above, a recent theoretical model can explain the infrared activity of the zone-edge magnon by considering the spin-exchange term $\vec{S}_i \cdot \vec{S}_j$ between the noncollinear spins as well as the local broken symmetry due to the orbital order or displacement of oxygen ions in the ab plane.[20,21] In this model, uniform electric field of light E^{ω} only along the a axis can give rise to the zone-edge magnon via the spin-exchange-coupled electric dipole $\vec{\pi}_{ij}(\vec{S}_i \cdot \vec{S}_j)$. Here, $\vec{\pi}_{ij}$ is the local electric dipole built-in between the ith and jth Mn sites. The higher-lying peak of electromagnon around 60 cm^{-1} in $TbMnO_3$ has been assigned by this model to this zone-edge magnon in the bc-spiral phase.[20,21] For the ab-spiral phase in $Eu_{1-x}Y_xMnO_3$, we may also consider this mechanism as the origin of far-infrared absorption because the essence of this model is the uncanceled electric-dipole activity in the noncollinear-spin structure and the ab-spiral structure in $RMnO_3$ also fulfils this condition; the spin-coupled dipole depends only on the inner product $\vec{S}_i \cdot \vec{S}_j$ and not on the direction of $\vec{S}_i(\vec{S}_j)$. On the basis of this assignment, the frequency shift from 73 $\mathrm{cm}^{-1}(x=0.3)$ to 59 $\mathrm{cm}^{-1}(x=0.45)$ with x (Fig. 4) may reflect the shift in the zone-edge energy of magnon dispersion. This model is also consistent with the disappearance of the absorption of electromagnon in the A-type AFM phase, whose slight spin noncollinearity along the c axis cannot give rise to the dipole activity of one-magnon excitation due to the lattice symmetry.

As shown in Fig. 4, this lower-lying peak of electromagnon is close to the frequency of the observed antiferromagnetic resonance in $H^{\omega} \| a$ configuration. The same tendency has also been observed for $TbMnO_3$,[31] $DyMnO_3$,[18] $Eu_{0.75}Y_{0.25}MnO_3$,[13] and $Gd_{0.7}Tb_{0.3}MnO_3$.[16] One possible candidate for this low-energy excitation could be magnon at $q=q_m$. This magnon at $q=q_m$ with a finite gap energy has been observed by inelastic neutron scattering in $TbMnO_3$,[10,11,30] and also by antiferromagnetic resonance.[13,16,18,19,31] However, the aforementioned exchange-striction model, or at least its simplest form, cannot account for the infrared activity of the magnon at $q=q_m$ and this issue should be clarified by future theoretical and experimental investigations.

Lastly, we consider the origin of the plateaulike absorption band observed in the collinear sinusoidal phase. In $TbMnO_3$, the magnon dispersion in the collinear sinusoidal phase has been observed from 12 to 65 cm^{-1} from the neutron-scattering experiments[10] whose energy range approximately coincides with the spectral range of the electric-dipole active magnetic excitations.[19] In $Eu_{1-x}Y_xMnO_3$, the absorption band appears below 100 cm^{-1} with strong electric-dipole activity even in the paraelectric materials ($x=0.1$ and 0.2). This excitation also shows the strong correlation with the lowest optical-phonon mode as shown in Figs. 7 and 8, implying the close analogy to the electromagnons in the spiral-spin phase. The model based on the noncollinear-spin structure[20,21] cannot straightforwardly explain the electromagnonlike absorption for the collinear-spin structures. The board continuumlike band might be interpreted in terms of the electric-dipole active two-magnon band, as the present authors speculated at the early stage of the research on electromagnon for $RMnO_3$.[16,18,19] However, the recent theoretical calculation has indicated that the one-magnon process in the noncollinear-spin state can give rise to the far strong electric-dipole activity than the two-magnon process, in particular, in the case of $RMnO_3$.[21] In this context, the spectral weight of this broad magnetic-excitation band in the collinear-spin state appears to exceed 1/3 of that of the electromagnon band in the spiral-spin state and hence cannot be explained by the two-magnon scenario. Considering the fact that the collinear-spin state locating adjacently to the spiral-spin state can be viewed as the superposition of the nearly degenerate *ab*- and *bc*-spiral states, the thermal excitation of the spiral-spin states in the averaged collinear-spin state is perhaps responsible for the strong and broad absorption band as observed.

VI. CONCLUSION

We have systematically investigated spectra of the electromagnons and their coupling with the optical phonons in $Eu_{1-x}Y_xMnO_3$ ($x=0.1$, 0.2, 0.3, 0.4, and 0.45). In the spiral-spin phase endowed with ferroelectricity, the absorption spectra of the electromagnon below 100 cm^{-1} consists of two bands, one around 20 cm^{-1} and another around 65 cm^{-1}. Among them, the higher-lying band can be assigned to the zone-edge magnon, which can be electrically activated by the $\vec{\pi}_{ij}(\vec{S}_i \cdot \vec{S}_j)$ term in the noncollinear spins $(\vec{S}_i \cdot \vec{S}_j)$ through the modulation of the local electric dipole $\vec{\pi}_{ij}$. The higher-lying band is observed to shift to lower energy with increasing the Y content x or equivalently with decreasing spin-exchange interaction; this is consistent with the above assignment, since the zone-edge magnon energy measures the magnitude of the exchange interaction. On the other hand, electromagnon completely disappears in the *A*-type antiferromagnetic phase. The intensity of the lowest optical phonon decreases in the collinear sinusoidal and spin-spiral phase, showing the anticorrelation with the spectral intensity of the electromagnons (in the spiral phase) or electric-dipole active broad continuum (in the collinear sinusoidal phase). At maximum, one half of the spectral weight of the electromagnon appears to originate from the lowest optical-phonon mode for $x=0.4$, indicating appreciable coupling between electromagnons (or their fluctuations) and specific lower-lying optical-phonon modes.

We thank S. Miyahara, M. Mochizuki, and N. Furukawa for fruitful discussion. This work was in part supported by Grant-in-Aids for Scientific Research (Grants No. 16076205 and No. 20340086) from the Ministry of Education, Culture, Sports and Technology (MEXT), Japan.

[1] T. Kimura, T. Goto, H. Shintani, K. Ishizaka, T. Arima, and Y. Tokura, Nature (London) **426**, 55 (2003).
[2] Y. Tokura, Science **312**, 1481 (2006); W. Eerenstein, N. D. Mathur, and J. F. Scott, Nature (London) **442**, 759 (2006); S.-W. Cheong and M. Mostovoy, Nature Mater. **6**, 13 (2007).
[3] T. Kimura, G. Lawes, T. Goto, Y. Tokura, and A. P. Ramirez, Phys. Rev. B **71**, 224425 (2005).
[4] H. Katsura, N. Nagaosa, and A. V. Balatsky, Phys. Rev. Lett. **95**, 057205 (2005).
[5] M. Mostovoy, Phys. Rev. Lett. **96**, 067601 (2006).
[6] I. A. Sergienko and E. Dagotto, Phys. Rev. B **73**, 094434 (2006).
[7] Y. Yamasaki, H. Sagayama, T. Goto, M. Matsuura, K. Hirota, T. Arima, and Y. Tokura, Phys. Rev. Lett. **98**, 147204 (2007).
[8] Y. Yamasaki, H. Sagayama, N. Abe, T. Arima, K. Sasai, M. Matsuura, K. Hirota, D. Okuyama, Y. Noda, and Y. Tokura, Phys. Rev. Lett. **101**, 097204 (2008).
[9] A. Pimenov, A. A. Mukhin, V. Yu. Ivanov, V. D. Travkin, A. M. Balbashov, and A. Loidl, Nat. Phys. **2**, 97 (2006).
[10] D. Senff, P. Link, K. Hradil, A. Hiess, L. P. Regnault, Y. Sidis, N. Aliouane, D. N. Argyriou, and M. Braden, Phys. Rev. Lett. **98**, 137206 (2007).
[11] D. Senff, N. Aliouane, D. N. Argyriou, A. Hiess, L. P. Regnault, P. Link, K. Hradil, Y. Sidis, and M. Braden, J. Phys.: Condens. Matter **20**, 434212 (2008).
[12] H. Katsura, A. V. Balatsky, and N. Nagaosa, Phys. Rev. Lett. **98**, 027203 (2007).
[13] R. Valdés Aguilar, A. B. Sushkov, C. L. Zhang, Y. J. Choi, S.-W. Cheong, and H. D. Drew, Phys. Rev. B **76**, 060404(R) (2007).
[14] A. Pimenov, A. Loidl, A. A. Mukhin, V. D. Travkin, V. Yu. Ivanov, and A. M. Balbashov, Phys. Rev. B **77**, 014438 (2008).
[15] N. Kida, Y. Takahashi, J. S. Lee, R. Shimano, Y. Yamasaki, Y. Kaneko, S. Miyahara, N. Furukawa, T. Arima, and Y. Tokura, J. Opt. Soc. Am. B **26**, A35 (2009).
[16] N. Kida, Y. Yamasaki, R. Shimano, T. Arima, and Y. Tokura, J. Phys. Soc. Jpn. **77**, 123704 (2008).
[17] J. S. Lee, N. Kida, S. Miyahara, Y. Takahashi, Y. Yamasaki, R. Shimano, N. Furukawa, and Y. Tokura, Phys. Rev. B **79**, 180403(R) (2009).
[18] N. Kida, Y. Ikebe, Y. Takahashi, J. P. He, Y. Kaneko, Y. Yamasaki, R. Shimano, T. Arima, N. Nagaosa, and Y. Tokura, Phys. Rev. B **78**, 104414 (2008).
[19] Y. Takahashi, N. Kida, Y. Yamasaki, J. Fujioka, T. Arima, R.

Shimano, S. Miyahara, M. Mochizuki, N. Furukawa, and Y. Tokura, Phys. Rev. Lett. **101**, 187201 (2008).
[20] R. Valdés Aguilar, M. Mostovoy, A. B. Sushkov, C. L. Zhang, Y. J. Choi, S.-W. Cheong, and H. D. Drew, Phys. Rev. Lett. **102**, 047203 (2009).
[21] S. Miyahara and N. Furukawa, arXiv:0811.4082 (unpublished).
[22] A. Pimenov, T. Rudolf, F. Mayr, A. Loidl, A. A. Mukhin, and A. M. Balbashov, Phys. Rev. B **74**, 100403(R) (2006).
[23] J. Hemberger, F. Schrettle, A. Pimenov, P. Lunkenheimer, V. Yu. Ivanov, A. A. Mukhin, A. M. Balbashov, and A. Loidl, Phys. Rev. B **75**, 035118 (2007).
[24] Y. Yamasaki, S. Miyasaka, T. Goto, H. Sagayama, T. Arima, and Y. Tokura, Phys. Rev. B **76**, 184418 (2007).
[25] T. Kimura, S. Ishihara, H. Shintani, T. Arima, K. T. Takahashi, K. Ishizaka, and Y. Tokura, Phys. Rev. B **68**, 060403(R) (2003).
[26] M. Mochizuki and N. Furukawa, J. Phys. Soc. Jpn. **78**, 053704 (2009).
[27] H. Murakawa, Y. Onose, F. Kagawa, S. Ishiwata, Y. Kaneko, and Y. Tokura, Phys. Rev. Lett. **101**, 197207 (2008).
[28] N. Abe, K. Taniguchi, S. Ohtani, T. Takenobu, Y. Iwasa, and T. Arima, Phys. Rev. Lett. **99**, 227206 (2007).
[29] B. Ferguson and X.-C. Zhang, Nature Mater. **1**, 26 (2002).
[30] D. Senff, P. Link, N. Aliouane, D. N. Argyriou, and M. Braden, Phys. Rev. B **77**, 174419 (2008).
[31] A. Pimenov, A. Shuvaev, A. Loidl, F. Schrettle, A. A. Mukhin, V. D. Travkin, V. Yu. Ivanov, and A. M. Balbashov, Phys. Rev. Lett. **102**, 107203 (2009).